

Dual-Salts Electrolyte to Effectively Reduce Impedance Rise of High-Nickel Lithium-Ion Batteries

Jianzhong Yang,^a Marco-Tulio Fonseca Rodrigues,^a Seoung-Bum Son,^a Juan C. Garcia,^a Kewei Liu,^a Jihyeon Gim,^a Hakim Iddir,^a Daniel P. Abraham,^a Zhengcheng Zhang^a and Chen Liao*^{a,b}

^a Chemical Sciences and Engineering Division, Argonne National Laboratory, 9700 South Cass Avenue, Lemont, Illinois, 60439, United States

^b Joint Center for Energy Storage Research, Lemont, Illinois, 60439, United States

Corresponding author: Chen Liao, liaoc@anl.gov, 630-252-4597

Abstract

Simply mixing several lithium salts in one electrolyte to obtain blended salts electrolyte showing synergistic effects has been demonstrated as a promising strategy to formulate advanced electrolyte for lithium metal batteries (LMBs) and lithium-ion batteries (LIBs). In this study, we report the use of dual-salts electrolytes containing lithium hexfluorophosphate (LiPF₆) and lithium difluorophosphate (LiDFP) in ethylene carbonate / ethyl methyl carbonate (EC/EMC) mixture and tested in layered high nickel LIB cells. LiNi_{0.94}Co_{0.06}O₂ was synthesized through a co-precipitation method and used as a representative high nickel cathode for the US DOE Realizing Next Generation Cathodes (RNGC) deep dive program. The ionic conductivity of dual-salts electrolyte can be maintained by controlling the amount of LiDFP. Techniques including ¹H NMR, XPS, ICP-MS, and differential voltage analysis (DVA) were used to understand the improved performance. The multifaceted benefits of using the dual-salts electrolytes

include 1) reduced transesterification, 2) formation of a stable cathode electrolyte interface, and 3) mitigation of cathode degradation at high voltages, especially stabilization of oxide particles during the H₂↔H₃ transformation.

Keywords: dual-salts electrolyte, high-nickel lithium-ion batteries, ionic conductivity, impedance rise, transesterification and transition metal dissolution

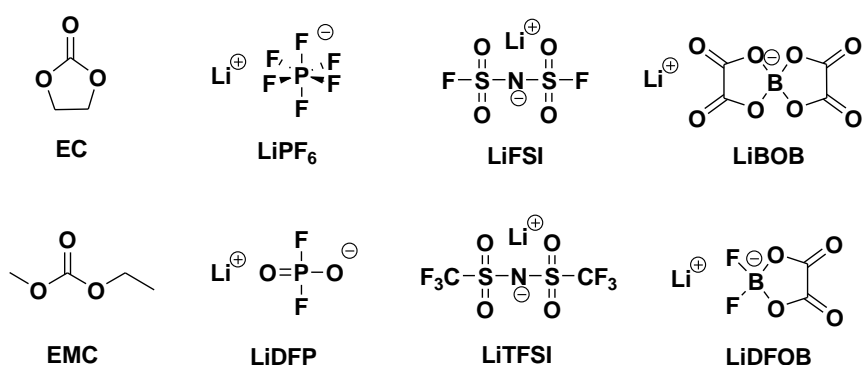
1. Introduction

Over the past few decades, rechargeable lithium-ion batteries (LIBs) have been successfully applied in consumer devices and have been considered as the most promising energy storage system. However, their large-scale application in hybrid electric or full-electric vehicles requires LIBs with sufficiently high energy density and rate capability.^{1,2} The high demand and growth of the LIBs put tremendous strain on the supply chain of some key elements, including cobalt (Co) and lithium (Li). Co is the “indispensable” component for the workhorse battery cathode material LiCoO₂ in consumer electronics due to its high volumetric energy density, however, Co is only mined in specific places such as Democratic Republic of the Congo (DRC), and unethical mining with use of child labor is associated with Co mining. Other transition metal analogs, such as manganese (Mn) and nickel (Ni), which can form isostructural transition metal oxide cathodes with a general formula of LiNi_xMn_yCo_zO₂ (x+y+z=1), are favored with their higher crustal abundance and well-established supplied chain. With sufficient high nickel content (x > 0.9), batteries retained the favorable high

energy density without the usage of Co. A new challenge has arisen: multiple phase transformations are associated with high nickel cathodes resulting in less stability and reversibility, and upon charge the formation of Ni^{4+} causes more detrimental electrolyte oxidation. Research exploring new electrolytes that can withstand the high operating voltage, but still maintain good cyclability and a high degree of safety, is needed.

The electrolyte, considered as the “blood” of LIBs, greatly affect their electrochemical performance and inherent safety. The traditional electrolyte for LIBs usually contains an organic carbonate solvent mixture, lithium salts, and additives for specific anode and cathode protection purposes. Both cyclic and linear carbonate solvents are used in the electrolyte; with ethylene carbonate (EC) and ethyl methyl carbonate (EMC) being the two most commonly used electrolyte solvents, as shown in Scheme 1. It’s also worthy to mention that these carbonate solvents are usually flammable, posing safety risks. Thus, battery research community had applied many strategies to realize their safe applications in LIBs.^{3,4} Several widely used lithium salts are also listed in Scheme 1. Among them, lithium hexafluorophosphate (LiPF_6) salt exhibits high ionic conductivity and good electrochemical performance in LIBs, but has two drawbacks: poor thermal stability and high moisture sensitivity.^{5,6} Lithium borate salts such as lithium bis (oxalato) borate (LiBOB) and lithium difluoro (oxalato) borate (LiDFOB) confer good thermal and chemical stability, but they are limited by their high cost and low solubility in organic carbonate solvents. Lithium imides salts like lithium bis(trifluoromethanesulfonyl) imide (LiTFSI) and lithium bis(fluorosulfonyl) imide (LiFSI) have the advantages of high thermal stability and resistance to hydrolysis.

However, their dilute aprotic electrolyte solutions are known to strongly corrode the Al current collectors at high voltages.^{7, 8}



Scheme 1. Chemical structures of carbonates and lithium salts commonly used in electrolytes for lithium-ion batteries

Current commercial electrolytes usually contain only a single lithium salt dissolved in a mixture of solvents, and a few electrolyte additives. Nevertheless, electrolyte compositions featuring multiple lithium salts at concentrations higher than those typically used for additives have been shown to achieve improved physical and electrochemical properties. For example, a dual-salts electrolyte containing 0.25M LiPF₆/0.6M LiBOB in an EC/DEC (diethyl carbonate) mixture achieved much higher thermal stability than an electrolyte containing only LiPF₆.⁹ Another dual-salts electrolyte composed of 0.8M LiFSI/0.2M LiDFOB in an EC/DEC mixture effectively suppressed Al corrosion caused by LiFSI salt.¹⁰ The blended-salts electrolyte with 1M LiDFOB/LiPF₆ (4:1 in an EC/PC(propylene carbonate)/DMC(dimethyl carbonate mixture)) in full cells with LiFePO₄/artificial graphite achieves much better cycling performance than the single LiPF₆ based electrolyte, especially at a high temperature of 65 °C.¹¹ Therefore, incorporating multiple salts to achieve a synergistic effect has become a promising strategy to improve performance of LIBs.

Recently, advanced lithium salts such as lithium difluorophosphate (LiDFP) have been reported by Yang *et al.* as electrolyte additives to modify the composition of the solid electrode interphase (SEI) layer, which inhibits side reactions between electrode and electrolyte and improves the cyclability of LIBs.¹²⁻¹⁵ However, LiDFP itself is not appropriate to be used as a standalone electrolyte salt, owing to its low ionic conductivity.¹⁶

The other key point here is the use of a representative high nickel cathode, $\text{LiNi}_{0.94}\text{Co}_{0.06}\text{O}_2$ ($\text{N}_{94}\text{C}_{06}$).¹⁷ Initially studied by Manthiram *et al.*, elimination of EC in the electrolytes improved significantly the performance of $\text{N}_{94}\text{C}_{06}$. When coupled with an EC free electrolyte, $\text{N}_{94}\text{C}_{06}$ exhibited long cycle life with a specific capacity reaching 235 mAh g^{-1} , high tolerance of thermal abuse, mitigated surface parasitic reactions with electrolyte, and less structural bulk cathode degradation.

Herein, we report the combination of LiDFP and LiPF_6 salt to form dual-salts electrolytes with a 1.2M total lithium salt concentration in an EC/EMC (3/7, wt/wt) mixture. It is worth mentioning that the structure of LiDFP resembles that of the *in situ* synthesized lithium oxyfluorophosphate salts,¹⁷ both of which are cathode protective agents for LIBs. By adjusting the content of LiDFP, high ionic conductivity of the electrolytes can be maintained, and the electrochemical performance of full cells containing the high nickel cathode $\text{LiNi}_{0.94}\text{Co}_{0.06}\text{O}_2$ ($\text{N}_{94}\text{C}_{06}$) and a graphite anode (Gr) can be improved. More importantly, the dual-salts electrolyte can inhibit the decomposition of electrolyte and mitigate the structural damage on cathode, and significantly suppress the impedance rise of cells during aging.

2. Experimental Section

2.1 Electrolyte and Electrodes: Gen2 electrolyte containing 1.2 M LiPF₆ in EC/EMC (3:7 w/w ratio), purchased from Tomiyama Chemical Industry (Japan), was used as the baseline electrolyte to compare with dual-salts electrolytes. The LiDFP salt was purchased from Hunan Chemfish Pharmaceutical Co., Ltd. Various ratios of dual-salts electrolytes were prepared by weighing out the masses of battery-grade LiPF₆ and LiDFP salts that were calculated to give the desired molarity and dissolving them in a EC/EMC (3:7 w/w ratio) mixture; the moisture level of the EC/EMC mixture was controlled to less than 20 ppm.

Ni_{0.94}Co_{0.06}(OH)₂ metal precursors were prepared by the coprecipitation method to form a uniform particle sized secondary particles. A solution containing stoichiometric 2M concentration of each component, NiSO₄·6H₂O, CoSO₄·7H₂O and MnSO₄·5H₂O, (all precursors from Sigma-Aldrich) was prepared and continuously pumped into a continuously stirred tank reactor (CSTR) that was filled with Nitrogen purged distilled water using a 4L batch reaction. During the feeding of the transition metal solution, an appropriate amount of an aqueous ammonia solution (5M) as a chelating agent was added to the reactor at a rate maintaining a fixed ratio between the transition metal salts and ammonium ions. The pH was also maintained at 11.05 with addition of an aqueous solution of 4M sodium hydroxide using a pH controller connected to the diaphragm metering pump. The temperature inside the reactor vessel was maintained at 55 °C, and the overhead stirrer was adjusted to 1000 RPM to achieve a homogenous reaction for a

preferred particle size distribution. The product of co-precipitated solution after 24 h of reaction was collected, and the precursor powder was obtained through repeated washing and filtering. The filtered precipitate was transferred to a convection oven and dried overnight under inert atmosphere to avoid any unwanted oxidation of the precursors. The $\text{Ni}_{0.94}\text{Co}_{0.06}$ oxide was prepared via a one-step calcination with a mixture of $\text{Ni}_{0.94}\text{Co}_{0.06}(\text{OH})_2$ and excess $\text{LiOH}\cdot\text{H}_2\text{O}$. The well-mixed powder was sintered at $680\text{ }^\circ\text{C}$ for 12 hours under a steady O_2 flow using a tube furnace with a wide stable hot-zone to avoid unwanted heat concentration deviation within the samples. The laminates of Ni-rich cathode and Gr-anode used in this study were provided by Argonne's Cell Analysis, Modeling and Prototyping (CAMP) facility. The $\text{LiNi}_{0.94}\text{Co}_{0.06}\text{O}_2$ (N94C06) cathode was made from a mixture of 90 wt% N94C06 powder, 5.0 wt% polyvinylidene fluoride binder (PVdF, Solvay, 5130) and 5 wt% conductive C45 carbon black particles (Timcal) coated on an aluminum current collector. The loading density for N94C06 was 8.64 mg/cm^2 . The graphite anode was composed of 92 wt% superior graphite (SLC1506T), 6 wt% PVDF binder (Kureha, 9300) and 2 wt% C45 carbon black particles (Timcal) coated on a copper current collector. The loading density was 6.38 mg/cm^2 . The microporous separator Celgard 2325 was used in the coin cell assembly. All electrodes and cell parts (except the separator) were dried at $110\text{ }^\circ\text{C}$ under vacuum prior to use, and the 2032-type coin cells were assembled in an argon-filled glovebox. The diameters of the cathode, graphite electrode, and separator were 14, 15, and 16 mm, respectively. The total amount of added electrolyte was $25\text{ }\mu\text{L}$ for each cell. In our study, at least three individual cells were tested for each electrolyte.

2.2 Electrochemical Measurement: Galvanostatic charge/discharge cycling between 3.0 and 4.2 V was conducted using MACCOR cyclers at 30 °C and a protocol described in Ref 18.¹⁸ Briefly, this protocol starts with five formation cycles at a C/10 rate, followed by a combination of modified hybrid pulse power characterization (HPPC), C/20, and 119 aging cycles at a C/3 rate. To monitor the area-specific impedance (ASI) change during the aging cycles, modified HPPC tests were inserted after every 20 cycles by using 10-s, 2C discharge pulses and 1.5C charge pulses. The currents are given as C-rates, where 1C is roughly 2.4 mA. The specific capacity of the cells was calculated from the weight of the lithiated oxide material in the cathode, by referring to the entire initial Li inventory of the cathode materials. The figure-of-merit (FOM) methodology, as described in Ref. 19, was used to quantitatively compare the performance of dual-salts electrolytes.¹⁹ Potentiostatic-hold experiments were performed by fully charging cells at 4.2 V and holding them at 4.2 V for 60 hours.²⁰ Rate tests were preceded by three formation cycles at the C/10 rate, followed by 5 cycles each at C/3, 1C, 2C, 5C, 2C, 1C and C/3. Ionic conductivity of electrolytes containing varied salt ratios were measured via AC impedance spectroscopy by using a custom-designed coin cell with a hollow Teflon disc of specific thickness and diameter (~12mm).

2.3 Postmortem characterization of harvested electrodes and electrolyte:

2.3.1 ¹H Nuclear Magnetic Resonance (NMR) analysis: The cycled cells were disassembled in an argon-filled glove box, and the cycled electrolyte was collected by dipping the electrodes and the separators in 1.0 mL CDCl₃. The resulting solutions were

subjected to ^1H NMR analyses. NMR spectra were obtained with a Bruker Avance III HD 300 MHz spectrometer, while the chemical shifts in parts per million (δ , ppm) were referenced to CDCl_3 at 7.26 ppm.

2.3.2 X-ray Photoelectron Spectra (XPS) characterization: XPS was performed by using a PHI 5000 VersaProbe II System (Physical Electronics) with a base pressure of 2×10^{-9} Torr. The cycled anodes and cathodes were harvested from the aged cells and carefully washed with DMC prior to measurement. The photoelectron spectra were obtained in the fixed analyzer transmission mode using an Al $K\alpha$ radiation ($h\nu = 1486.6$ eV, 100 μm beam, 25W) with Ar^+ and electron beam sample neutralization. XPS spectra were aligned to the graphitic carbon at 284.5 eV.

2.3.3 Inductively Coupled Plasma - Mass Spectra (ICP-MS) characterization: To quantitatively evaluate transition metal dissolution in the aged cells, the cycled anodes were rinsed, transferred to a quartz beaker, and burned in a furnace at 700 $^\circ\text{C}$ for 12 h to remove organic constituents and carbon. The ash was refluxed with a mixture of nitric and hydrochloric acids at 220 $^\circ\text{C}$ for 1 h, and the solutions were diluted with water. The samples were analyzed using inductive coupled plasma-mass spectrometry (ICP-MS) to determine the transition metal concentrations that were referred to the weight of the anode. Measurements were made using a PerkinElmer NexION 2000 ICP Mass Spectrometer calibrated with the NIST traceable standards.

2.3.4 Atomistic modeling calculations

The calculations use density functional theory (DFT) as implemented in the Vienna Ab

Initio Simulation Package (VASP).^{1,2} The exchange-correlation potentials are treated by the generalized gradient approximation (GGA) parametrized by Perdew, Burke, and Ernzerhof (PBE).³ The interaction between valence electrons and ion cores is described by the projected augmented wave (PAW) method.⁴ Furthermore, the GGA+U scheme is used for applying the on-site correlation effects among 3d electrons of the TMs.⁵ The wave functions are expanded in the plane wave basis up to a kinetic energy of 500 eV. All the ions will be allowed to relax until the total energy differences were no more than 0.003 eV. Bulk solvent effects were accounted for by using an implicit solvation model as implemented in VASP.^{6,7}

3. Results

The composition of the Ni₉₄Co₀₆ oxide was confirmed as Li_{1.06}Ni_{0.94}Co_{0.06}O₂ by ICP-MS (Inductively Coupled Plasma - Mass Spectrometry) analysis. A Rietveld refinement analysis of the X-ray diffraction (XRD) pattern of the as-prepared material (not shown) revealed that the pure R-3m structure can be indexed without presence of any impurities. Li⁺/Ni²⁺ cation mixing was calculated to be 1.29%, which is far lower than values reported in the literature for pristine oxides with the same composition.¹⁷

The ionic conductivity of the electrolyte can significantly affect the electrochemical performance of LIBs. As mentioned in the introduction, pure LiDFP electrolyte has low ionic conductivity, which hinders its application as an electrolyte for LIBs. Therefore, we first evaluated the ionic conductivity of electrolytes containing varied salt ratios via AC impedance spectroscopy by using a custom-designed coin cell

with a hollow Teflon disc of specific thickness and diameter. The ionic conductivity of each electrolyte formulation was determined from 10 to 60 °C, and the results are depicted in Fig. 1A. Clearly, a concentration of LiDFP, such as 0.1 M, does not significantly change ionic conductivity of the electrolyte as compared with a pure LiPF₆-based solution, such as Gen2. However, further increase in LiDFP content lowers ionic conductivity of the dual-salts electrolyte. Therefore, the amount of LiDFP should be carefully controlled when preparing the dual-salts electrolyte.

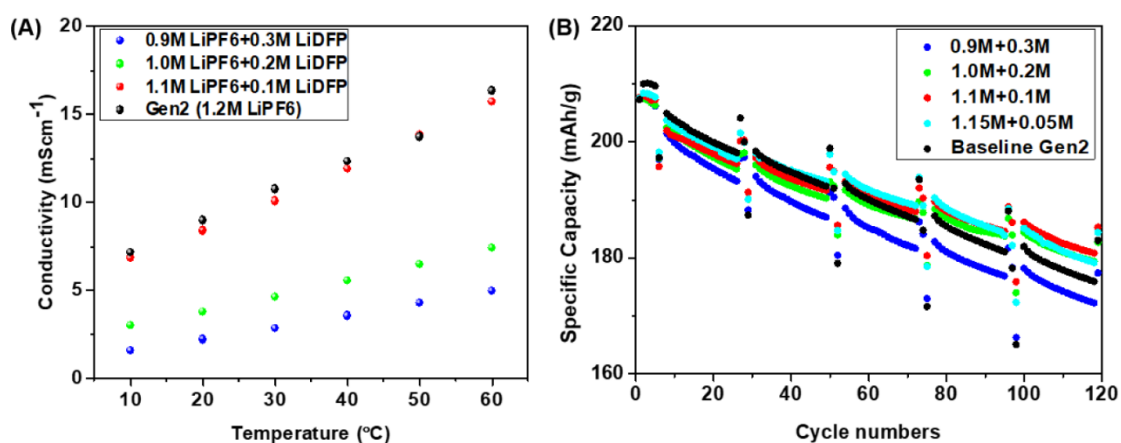


Figure 1. (A) Ionic conductivity of electrolyte with varied salt ratios. Addition of LiDFP to the electrolyte leads to a non-linear decrease in ionic conductivity. (B) Specific discharge capacity of cells with varied electrolyte ratios during aging cycles. The legend shows the concentration of LiPF₆ and LiDFP, respectively.

Electrochemical performance of the baseline electrolyte and the dual-salts electrolytes with varied salt ratios is illustrated in Fig. 1B, and some important metrics of cell performance are summarized in Table 1. The discontinuities of each curve in Fig. 1B were caused by the rate change (1C and C/10) after each HPPC sequence, performed every 20th cycle during the aging cycles. The cells containing the various

electrolytes were denoted as Gen2 cells (1.2 M LiPF₆) and 1.15M + 0.05M, 1.1M + 0.1M, 1.0M + 0.2M or 0.9M + 0.3M, which indicate the concentration of LiPF₆ and LiDFP, respectively. As shown in Fig. 1B, the cells with dual-salts electrolyte containing 0.2M LiDFP or less exhibit better electrochemical performance than Gen2 in terms of specific discharge capacity retention up to 119 cycles, while increasing LiDFP to 0.3M leads to worse electrochemical performance. Note (see Fig. 1) that the dual-salts electrolyte with 0.2M LiDFP exhibited a significant decrease in ionic conductivity, however, the synergistic effect of dual-salts compensates for the loss of ionic conductivity, providing better cell performance at this LiDFP condition. Apparently, further increasing the amount of LiDFP in the dual-salts electrolyte results in inferior cell performance, as shown by the 0.9M + 0.3M cells. Combining the results in Fig.1 and Table 1, the optimal salt ratio we found in our study is represented by the cells with 1.1M LiPF₆ and 0.1M LiDFP, which have the highest capacity retention and higher average coulombic efficiency after 119 cycles.

The FOM approach was used to quantitatively evaluate the benefits of dual-salts electrolyte.¹⁹ The FOMs are defined as the projected cycle number at which a given cell metric (energy density or power density) reaches 80% of the initial value exhibited by the baseline electrolyte (Gen2). Energy FOMs were determined by linear extrapolation of discharge capacities at the five C/10 performance checks in our protocol. As shown in Table 1, appropriate dual-salts compositions can increase the energy FOM by 25% (from 173 to 184, 196, and 215 for 0.05, 0.2, and 0.1M LiDFP, respectively) which is a significant improvement in cell performance. Note that our test

protocol was designed to accelerate cell aging by including a 3-hour voltage hold at the top-of-charge, and that the cycle life of our cells would be higher if simply tested using constant-current cycling.

Table 1. Electrochemical Performance Summary of the Dual-salts Electrolytes and Baseline Electrolyte.

Electrolyte		Gen2	1.15+0.05	1.1+0.1	1.0+0.2	0.9+0.3
1st cycle	charge	242.2 ± 2.3	239.6 ± 0.1	241.0 ± 0.9	240.6 ± 1.7	240.5 ± 0.6
specific	discharge	207.3 ± 2.5	207.8 ± 0.0	207.7 ± 0.6	206.9 ± 0.6	207.4 ± 0.3
capacity, ^a	% loss	14.4	13.3	13.8	14.0	13.8
Discharge	initial ^b	210.1 ± 0.8	208.3 ± 0.7	207.7 ± 0.8	206.4 ± 1.2	207.2 ± 0.3
specific	final ^b	183.0 ± 2.9	184.4 ± 1.7	185.3 ± 1.7	183.3 ± 3.5	177.4 ± 2.1
Capacity retention (%)		87.1 ± 1.5	88.5 ± 0.5	88.9 ± 0.5	87.3 ± 1.2	85.6 ± 0.1
Average Coulombic Efficiency		99.78	99.76	99.79	99.76	99.71
Figure of	energy density	173	184	215	196	161
merit ^c	power density	19	50	131	105	43
ASI, ^d	initial	21.9 ± 0.4	19.1 ± 0.5	19.1 ± 0.1	20.3 ± 2.5	22.1 ± 1.2
	final	40.4 ± 2.9	30.5 ± 1.6	25.8 ± 0.0	26.8 ± 0.5	35.3 ± 0.7
$\Omega \cdot \text{cm}^2$	increase	18.5	11.4	6.7	6.5	13.2

a. Formation cycles at a C/10 rate;

b. The “initial” and “final” correspond to 3rd cycle and 119th cycle, respectively;

c. Number of full cycles to reach 20% loss of energy density and power density, relative to the value of the first cycle of the baseline cells under identical cycling conditions;

d. Full-cell ASI determined by using HPPC method; details can be found in experimental section. Average values and standard deviations for two or three independent measurements are given.

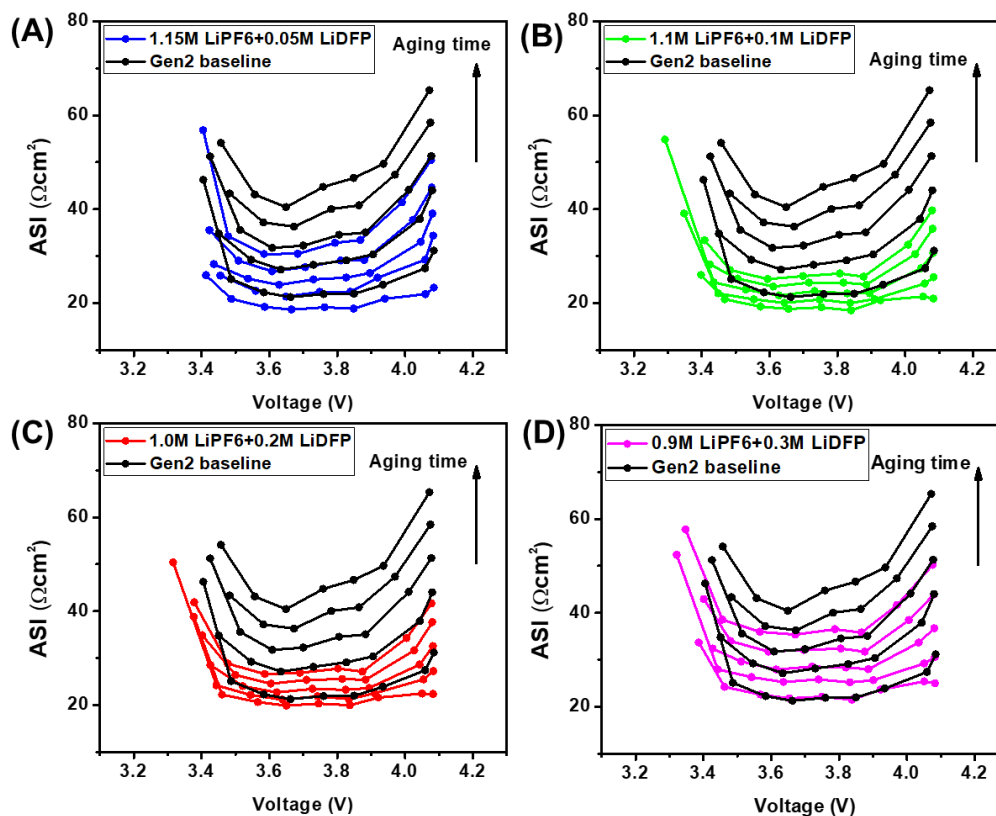


Figure 2. Area-specific impedance (ASI) for $N_{94}C_{06}$ //graphite cells with dual-salts electrolytes having varied salt ratios vs. baseline Gen2 electrolyte: (A) 1.15M + 0.05M, (B) 1.1M + 0.1M, (C) 1.0M + 0.2M, (D) 0.9M + 0.3M. From bottom to top, the traces in each graph correspond to the ASI measured after 7, 30, 53, 76, and 99 cycles, respectively.

The clearest benefits of these dual-salts electrolytes are found in cell impedance. Area-specific impedances (ASI) were measured from charge and discharge pulses performed at various voltages every 20 cycles in our test protocol. Only the ASI measured from discharge pulses are shown. ASI as a function of voltage is shown in Fig. 2, and detailed information on the initial and final HPPC sequences is summarized in Table 1. Compared to Gen2 cells, the dual-salts electrolyte cells all displayed

significantly less impedance rise; 1.1M + 0.1M cells and 1.0M + 0.2M cells showed the least impedance rise, i.e., about 30 % of the impedance rise found in baseline cells. Experiments in a 3-electrode cell (Fig. S1) indicated that the impedance rise during aging of the baseline cell originated from the cathode, suggesting that the dual-salts compositions are stabilizing the surface of positive electrode. Also note that, despite the lower ionic conductivity of dual-salts electrolytes (Fig. 1A), the initial impedance of cells with these electrolytes was generally lower than cells with Gen2 electrolyte, suggesting that the films formed at the surface of the cathode and anode are inherently more conducive to Li^+ ion transport. On the other hand, the cycling performance of these lithium ion batteries, especially Energy FOM, depends not only on ASI (which contributes more to power of the cell and cathode degradation under high voltages), but also on a matrix of conditions, including the quality of the SEI, dissolution of the transition metal, the lithium inventory trapping, etc, hence the difference of concentration of LiDFP (0.1 M vs 0.2 M) leads to slight change in Energy FOM.

The lower impedance rise observed with dual-salts electrolyte can be partly due to lower electrolyte reactivity at the surface of the cathode. To confirm this hypothesis, a potentiostatic-hold experiment was performed for cells with dual-salts electrolytes having varied ratios. When cells are fully charged and held at high potential for hours, the resulting leakage currents during the voltage hold can reflect parasitic reactions on the cathode surface.²¹ In our study, cells with varied-ratio dual-salts electrolytes or baseline electrolyte were fully charged at 4.2 V and held at 4.2 V for 60 hours; the leakage currents were recorded and plotted vs. holding time as shown in Fig. 3A.

Clearly, cells with dual-salts electrolyte displayed lower leakage currents than cells with baseline electrolyte, suggesting less decomposition of the electrolyte and more stable interphase formation with dual-salts electrolytes. The 1.1M + 0.1M cells had the lowest leakage currents, consistent with the lowest impedance rise and best cell performance.

The rate capability is an important parameter of LIBs, and it is greatly affected by the electrolyte used. Rate tests for cells with varied-ratio dual-salts electrolytes were performed at rates ranging from C/10 to 5C and compared with the Gen2 baseline electrolyte as shown in Fig. 3B. Cells with dual-salts electrolyte displayed higher charge/discharge capacity than baseline-electrolyte cells at rates between C/3 and 2C. When the rate increased to 5C, the cells with dual-salts electrolyte exhibited lower charge and discharge capacities, which decreased as the content of LiDFP salt increased. We speculate that this might be caused by lower ionic conductivities of dual-salts electrolytes, with the bulk properties, such as ionic transport of the electrolyte, playing the dominant role at high cycling rates. At a lower rate (less than 5C), the less-resistant electrolyte/electrode interface generated by the dual-salts electrolyte might compensate for the bulk properties of the dual-salts electrolyte, resulting in better rate capability than the baseline electrolyte.

The high rate testing does not contradict the previous low rate testing at C/3 (Fig. 1), since the high currents associated with higher rate can cause numerous exacerbated side reactions with consequent cross over and trapping of the Li inventory of the deleterious species with those high currents, which would be reflected as the exacerbated loss of capacity with higher rates. These side reactions, however, may not

be present at a low rate ($C/3$).

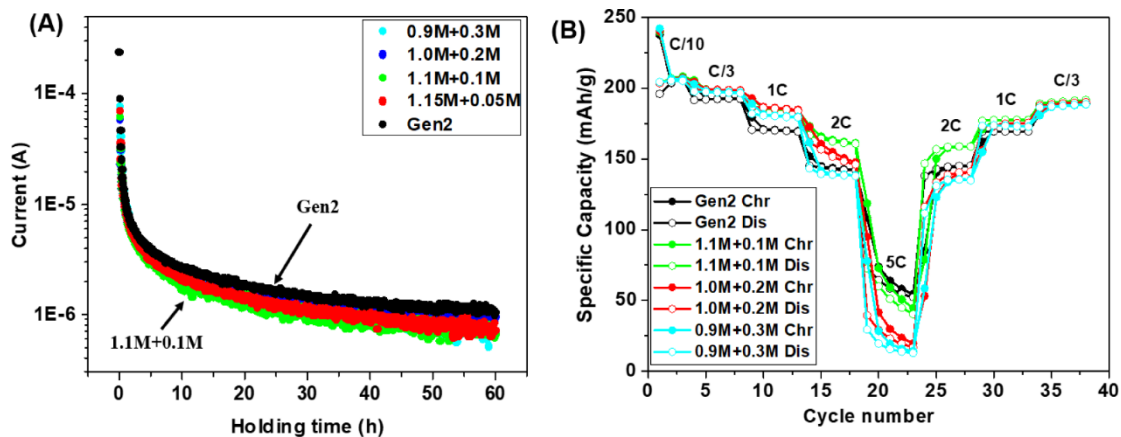


Figure 3. (A) Leakage currents of cells with electrolytes having varied dual-salts ratios and with baseline electrolyte. The legend shows the concentration of LiPF_6 and LiDFP , respectively. (B) Rate test of varied dual-salts electrolytes and baseline electrolytes.

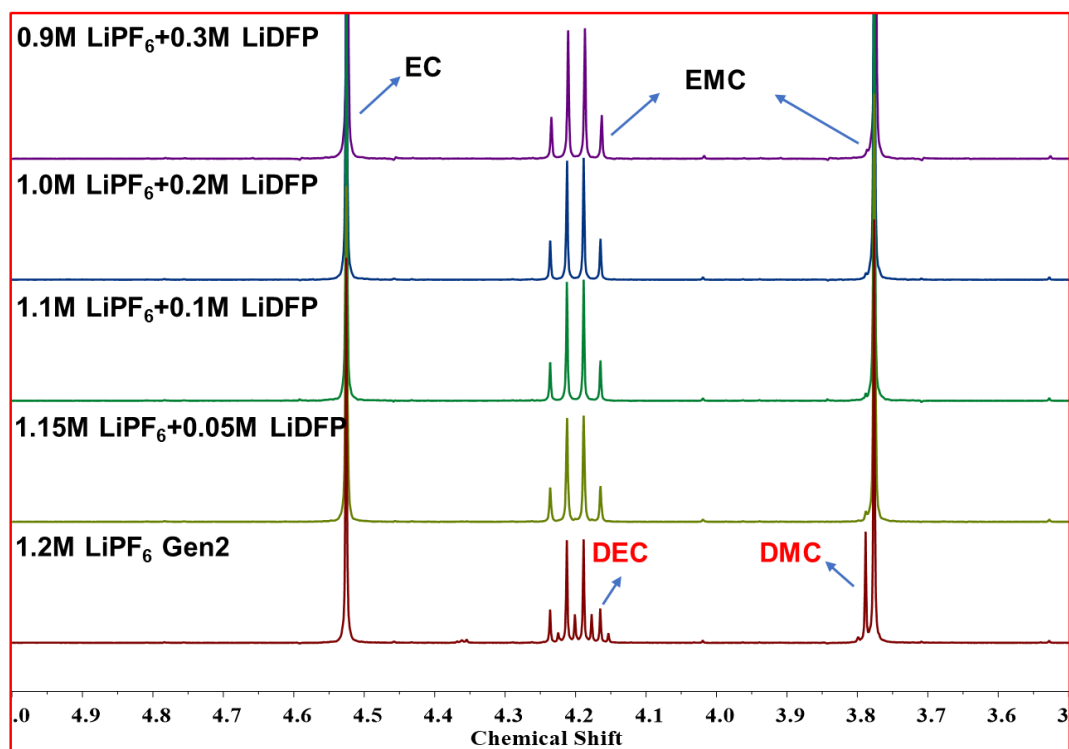


Figure 4. ^1H NMR spectra of electrolytes extracted from cycled cells, in CDCl_3 .

To examine mechanisms that lead to the superior cycling performance of cells

with dual-salts electrolyte, ^1H NMR, XPS and ICP-MS were used to probe the changes in the cycled electrolyte and the aged electrode surface. ^1H NMR spectroscopy was used to characterize the composition change of cycled electrolyte, as shown in Fig. 4. It has been reported that EMC can undergo transesterification reactions to produce DMC and DEC in LIBs, most likely via a reductively initiated mechanism, where the lithium alkoxides generated from either cyclic carbonate or linear carbonate molecules nucleophilically attack other carbonate molecules. As the initial reduction occurs at the anode surface, the amount of DEC and DMC indirectly reflects how well the anode has been passivated.²²⁻²⁴ Transesterification byproducts (DMC and DEC) were detected in the ^1H NMR spectra from Gen2 cells but not in the ^1H NMR spectra from cycled dual-salts electrolytes, suggesting the suppression of transesterification reactions and excellent passivation of the graphite anode upon addition of LiDFP to the cell.^{25,26}

The changes in surface chemical composition of cycled anodes and cathodes were probed by XPS characterization, and the C 1s, O 1s, F 1s and P 2p regions are plotted in Fig. S2 and Fig. S3 for anodes and cathodes, respectively. For the cycled anodes, the suppression of peaks at 291 eV ($-\text{CF}_2-$) and 285 eV (C-C) from PVDF binder suggests that passivated films formed on graphite, while the slight composition changes in C=O and C-O in the C 1s and O 1s region were caused by the formation of Li_2CO_3 , LiRCO_3 , or polyethylene glycol (PEG) species.²⁷ A striking difference was found in the F 1s region: a higher LiF content was observed on the anode surface cycled in dual-salts electrolytes with higher molar ratios of LiDFP, since the LiDFP salt introduced more F^- into the SEI.²⁸ The resulting higher LiF content could explain the

better passivation properties of the SEI formed by the dual-salts electrolyte, owing to the insulating character of LiF, which prevents electron tunneling and inhibits SEI growth.²⁹ This finding is consistent with the fact that no detectable transesterification reactions were found in dual-salts electrolyte. Since the stiffness of SEI increases as the contents of inorganic species increases, high content of inorganics might reduce the mechanical stability of SEI.³⁰ Therefore, the content of LiF in SEI must be optimal to reach a balance between electrochemical properties and mechanical stability. This agrees with the observation that the highest LiDFP salt ratios did not render best cell performance, and compromises were observed when the concentration of LiDFP reached a concentration equal or above 0.2 M.

For all the cycled cathodes in the C 1s and O 1s region, the amplitudes of the peaks at 285 eV and 291 eV originating from the PVDF binder was suppressed, suggesting that the deposition of a surface layer occurred during testing. Additionally, cycled cathodes with dual-salts electrolytes exhibited higher C-O content, suggesting that higher contents of PEG species may be present at the surface. Qian et. al proposed an oxidatively-catalyzed PEG formation mechanism, where EtOLi is transported from the anode to the cathode and further attacks EC to form PEG at the cathode side.²⁷ This polymeric film might contribute to the formation of more stable interphase on cathode surface, since it could potentially improve the mechanic properties of cathode interphase.

The improved protection of cathode surfaces by dual-salts electrolytes can also be indirectly probed by quantifying the amount of transition metal ions that are etched

away from the oxide and deposits on the anode surface. Fig. 5 shows the total Co and Ni content at the anode surface as measured by ICP-MS of cycled electrodes tested with the baseline and dual-salts electrolytes. Addition of LiDFP clearly correlates with lower levels of the dissolution in the transition metal Co and Ni, which decreases, respectively, by 76% and 54%. It is noteworthy that the reduction of transition metal loss agrees well with their improved cell performance associated with dual-salts electrolytes (Fig. 1B and Table 1). For example, Co dissolution was suppressed the most in electrolyte with 0.1M LiDFP, while Ni dissolution in electrolyte with 0.1M LiDFP was very close to that of electrolyte with 0.2M LiDFP. Cobalt is known to play a more important role in stabilizing the layered structure of cathode. Therefore, electrolyte with 0.1M LiDFP might be more beneficial to keep the layered structure of cathode, which should explain its slightly better performance than electrolyte with 0.2M LiDFP. On the other hand, electrolyte with 0.2M LiDFP had the least Ni dissolution, which might explain its comparable cell performance with electrolyte with 0.1M LiDFP, though its ionic conductivity is much less than electrolyte with 0.1M LiDFP.

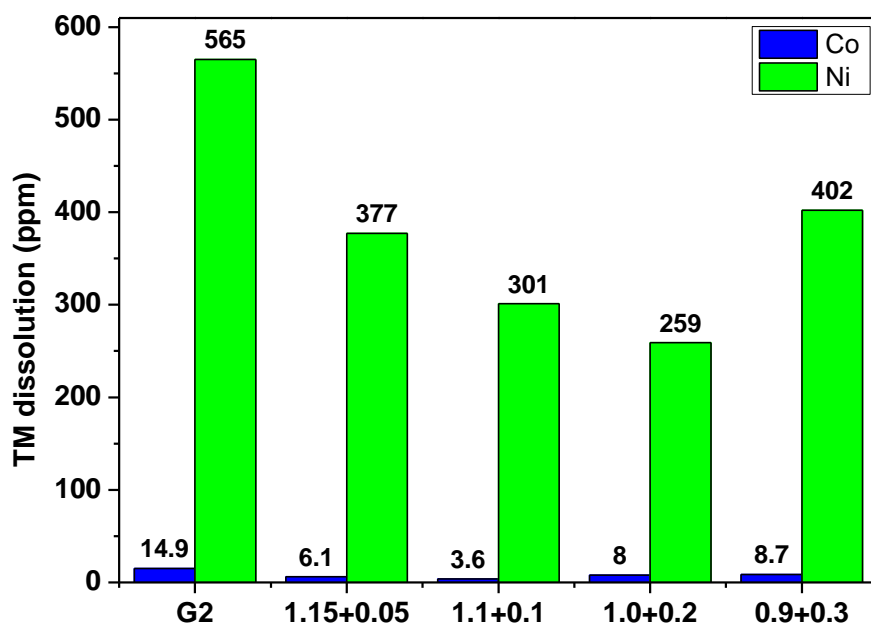


Figure 5. ICP-MS analysis of cycled anodes with varied dual-salts electrolyte and baseline electrolyte. The labels on the x-axis show the concentration of LiPF_6 and LiDFP , respectively.

Many of the characterization techniques discussed above indicate that the dual-salts electrolytes play a role in modifying the cathode surface. To achieve a mechanistic understanding of the physical and electrochemical evidence presented here, we have performed DFT calculations to study the interaction of LiDFP with the surface of a Ni-rich cathode. To simplify our model, a slab surface of pure LiNiO_2 is used in the simulation to represent Ni-rich compositions, such as $\text{Ni}_{94}\text{Co}_{06}$. Since previous work determined that the (012) facet is the most abundant and reactive NMC surface,⁸ we used the (012) facet as the prototype surface in all our calculations. Moreover, we used ab-initio molecular dynamics (AIMD) to explore the configuration space of the molecules over the surfaces. We tested several adsorption configurations to find atomic

positions that minimized the adsorption energy on the fully lithiated surface. The final state of our simulation indicates a chemical transformation of the salt at the cathode surface, where the salt LiDFP is converted to lithium monofluorophosphate (LiMFP). The chemical reaction presented a difference in energy between products and the reactants of -0.11 eV/f.u., indicating a thermodynamically favored reaction. Additionally, the reaction seems to have a negligible activation barrier, since it occurred spontaneously during the energy minimization procedure. Fig. 6 shows a schematic representation of the final product absorbed on the surface. The final state shows an exchange between one of the fluorine ions originally in the LiDFP molecule and a sub-surface oxygen atom from the LiNiO_2 lattice. This configuration is stabilized by the electrostatic interaction created by the negatively charged monofluorophosphate group and the F-doped oxygen lattice. The stability of this system could explain the improved electrochemical performance of the dual-salts system, with the monofluorophosphate playing the role of a passivating agent, by preventing further surface reactions, hence helping decrease the impedance rise during cycling. The interchange between F from the LiDFP and O from the cathode surface, also works as surface F-doping mechanism that would reduce further surface reactivity.

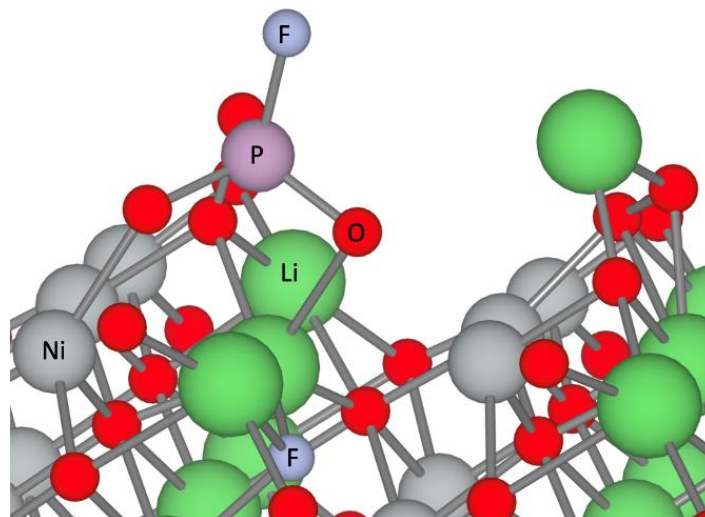


Figure 6. Ball and stick representation of lithium monofluorophosphate adsorbed at the (012) surface of a LiNiO_2 . One fluorine ion from the original lithium difluorophosphate salt is shown incorporated in the subsurface oxygen lattice. Blue spheres represent F ions, purple spheres represent P ions, grey spheres represent Ni ions, green spheres represent Li ions and grey sticks represent chemical bonds.

4. Discussion

Our work shows that LiDFP can be useful not only as an electrolyte additive, but also as a co-salt with LiPF_6 . Although the design of dual-salts system has been centered on lithium metal batteries (LMBs) and not LIBs, this study demonstrates that such an approach to electrolyte development can benefit the latter chemistry as well.

The XPS studies indicate that dual-salts electrolytes lead to a graphite SEI that is enriched in LiF (Fig. S2). However, the main mechanisms of SEI formation appears to remain unchanged, as the features in the dQ/dV curves of the first charge (Fig. S4) indicate that the main reduction events occur at a same potential of ~ 2.9 V vs. Li/Li^+

for both the baseline and dual-salt electrolytes. The improvements in anode passivation with dual salts are also indicated by the lack of transesterification of EMC in the electrolyte, as the access to electrons needed for the initial reductive step is effectively denied by the SEI.

Despite the evidence for significant enhancements in anode passivation, actual gains in capacity retention are modest (Fig. 1B and Table 1), suggesting that losses of Li^+ inventory to the SEI of graphite may not be the only dominant mechanism of performance fade in these cells. Indeed, many Ni-rich oxides have been reported to suffer severe capacity fade when delithiated beyond ~ 4.2 V vs. Li/Li^+ , as the $\text{H2} \leftrightarrow \text{H3}$ transition is accompanied by large changes in the lattice parameters.³¹ The excessive strain in the oxide particles upon charging lead to the formation of intergranular cracks,³² creating domains that are electronically isolated from the electrode matrix and become electrochemically inactive. The irreversibility caused by this $\text{H2} \leftrightarrow \text{H3}$ transition can be observed for Gen2 cells from the shortening of the dQ/dV peaks observed at ~ 4.1 V during charging of the full-cells (Fig. 7a).³² Peaks associated with other transitions in the cathode (~ 3.8 V) remain nearly unchanged, indicating that the capacity fade could be associated with a specific inactivation of electrochemistry at high voltages. Such losses of active material capacity will contribute to the overall capacity fade experienced by the cells.

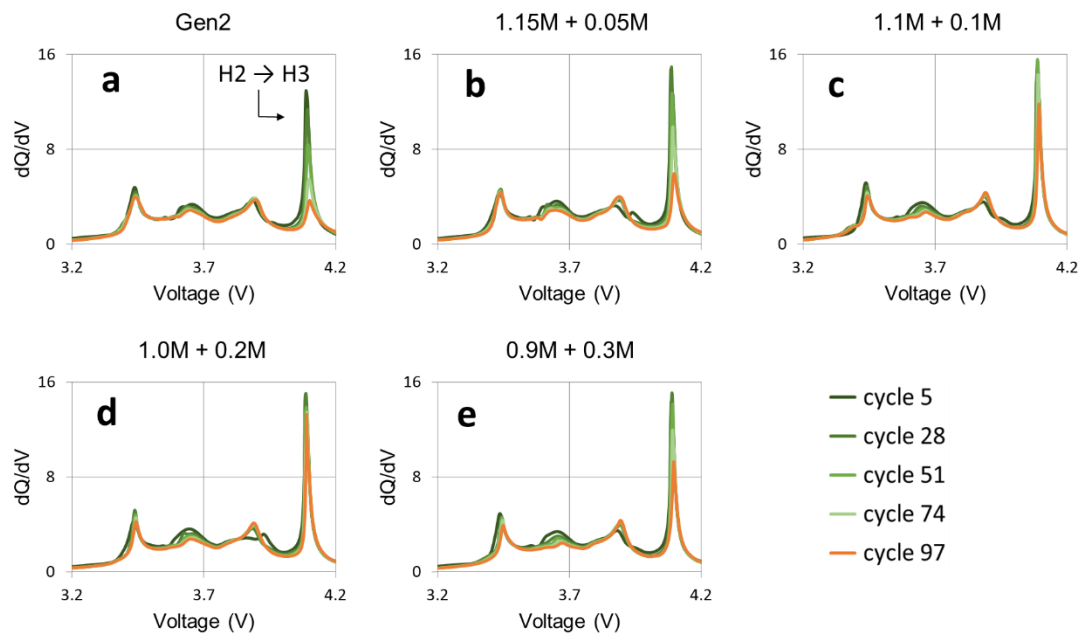


Figure 7. dQ/dV curves of C/10 charges of cells with baseline Gen2 electrolyte (a) or containing the dual-salts electrolytes 1.15M + 0.05M (b), 1.1M + 0.1M (c), 1.0M + 0.2M (d) or 0.9M + 0.3M (e), indicating the concentration of LiPF₆ and LiDFP, respectively. The legend at the bottom-right portion of the figure applies to all panels. Dual-salts electrolytes lead to improved reversibility of H2 ↔ H3 transitions of the cathode.

When dual-salts electrolytes are used, however, the peaks corresponding to the H2 → H3 transitions present a much slower decay over cycling (Fig. 7b-e). At certain concentrations of LiDFP (0.1M and 0.2M, especially the latter), the peak amplitude remains nearly unchanged at the end of testing, suggesting that these electrolyte formulations can have a remarkable effect on attenuating the detrimental effects of lattice “breathing”. Unsurprisingly, these compositions are also the ones that exhibited the most benefits to the capacity retention and impedance rise of these cells (Fig. 1 and Fig. 2). The baseline Gen2 electrolyte system, being more reactive, is more prone to

develop microcracks from the surface. Microcracks could lead to partially isolated particles that may lag behind in the charging process—given their local higher impedance. Hence, local state of charge heterogeneities can manifest as a two-phase H2/H3 mix at high state of charge, as reported before.¹⁷ Moreover, the smaller extent of the phase transformation in the dual-salts systems would attenuate the H2→H3 transitions dQ/dV peak. At optimal ratio of LiDPF/LiPF₆, the decreased reactivity of the dual-salts systems would mitigate the formation of cracks and the collateral performance decline. Therefore, electrolyte engineering can help mitigating what has been previously believed to be the intrinsic shortcomings of Ni-rich cathodes.

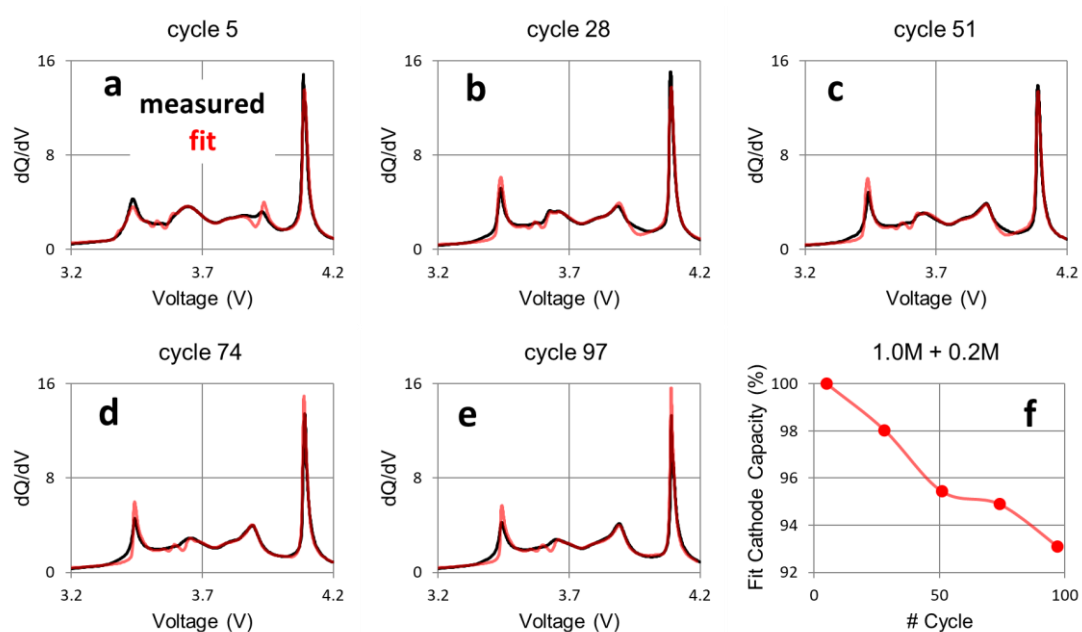


Figure 8. Differential voltage analysis (DVA) for the full-cells containing the dual-salts electrolyte with 1.0M LiPF₆ and 0.2M LiDFP. (a-e) Experimental dQ/dV curves at the indicated C/10 cycles are shown in black, while simulated traces obtained from fitted profiles are shown in red. The main features of the data are accurately captured by the model. (f) Retention of accessible cathode capacity obtained from DVA analysis.

~7% of cathode capacity is lost at the end of testing.

While Fig. 7 indicates that LiDFP helps mitigating some issues of these $\text{Ni}_{94}\text{Co}_6$ oxides, it does not solve all of them. To determine the origin of the capacity loss, we used a complementary advanced electrochemical analysis for mechanistic understanding: differential voltage analysis (DVA). DVA consists of “transforming” dV/dQ profiles from cathode and anode half-cells and combining them to reproduce dV/dQ curves observed for the full-cells (see Figure S5). The specific types of transformations needed for reproducing the data are related to the physical modes of capacity loss, enabling inferences about mechanisms of cell failure.³³

Since DVA is based on the profiles of unaged electrodes, the irreversible changes highlighted in Figure 7 preclude its full application to most of the samples studied here. Indeed, when comparing the dQ/dV traces of the profiles simulated by DVA with equivalent experimental data, an overestimation of the peak associated with $\text{H2} \rightarrow \text{H3}$ transitions is always observed at latter cycles (Figures S6-S9). The only exception is the electrolyte containing 0.2M LiDFP: the reversibility of the $\text{H2} \rightarrow \text{H3}$ transition in such cells is high enough (Fig. 7d) to allow DVA to be informative on the accessibility to cathode capacity as the cell ages. Results from DVA of these cells are shown in Fig. 8 for the C/10 charge cycles along the test protocol. Black lines are experimental dQ/dV profiles, while red traces are dQ/dV curves constructed using the “simulated” full-cell profile after performing DVA. While both dV/dQ and dQ/dV can be simulated from the DVA results, we opted for showing dQ/dV curves instead of the

dV/dQ as the former are more familiar to most battery scientists. The main features observed in the experimental data can be properly captured by the model, which assumes that the accessible capacity in the cathode decreases as shown in Fig. 8f. After 97 cycles, ~7% of the cathode capacity is lost; note that these full cells lost a total of ~13% of capacity during testing (Table 1). Hence, although the dual-salts electrolyte can drastically improve the reversibility of cathode reactions at high voltages, it does not fully prevent a decay in cathode capacity over repeated cycles.

While the mechanisms that favor the reversibility of high-voltage phase transitions assist in minimizing impedance rise, our study indicates that other sources are equally relevant. Reactivity of the electrolyte with the cathode surface is mitigated with dual-salts electrolytes, as we illustrate using voltage holds (Figure 3A). Our DFT calculations further suggest that part of this protective effect could originate from spontaneous fluorination of the sub-surface layers of the oxide and conversion of the LiDFP to LiMFP, which remains absorbed at the surface, preventing other reactions from happening. XPS data also indicates the enrichment of polymeric species (Fig. S3). All in all, the final surface chemistry of the cathode is clearly affected by addition of LiDFP as a co-salt to the electrolyte. All these changes ultimately contribute to minimizing the impedance rise as the cell ages (Fig. 2).

5. Conclusion

In this study, we found that incorporating LiDFP as a secondary salt with LiPF_6 in an EC/EMC (3/7, wt/wt) mixture to form a dual-salts electrolyte can improve the

electrochemical performance of high voltage LIBs employing Ni-rich cathodes. By controlling the amount of LiDFP, the ionic conductivity of the dual-salts electrolyte can be maintained. The dual-salts electrolyte with optimal ratios can improve the electrochemical performance of LIBs and effectively suppress the impedance rise of cells during aging via the formation of a stable cathode interface and mitigate the structural damage to cathode particles. While benefits conferred by dual-salts electrolytes are undeniable, DVA data from our accelerated aging tests suggest that the losses of cathode capacity can still be significant after extended exposure to high voltages. Nevertheless, our work shows that electrolyte engineering is essential to enable the adoption of Ni-rich cathodes.

Supporting Information

The Supporting Information is available free of charge on the ACS Publication website, including ASI data of 3-electrode cell, XPS data of cycled electrodes, dQ/dV profiles and DVA of cells with varied dual-salts electrolyte.

CRedit authorship contribution statement

Jianzhong Yang: Experiment design, Data collection and analysis, Writing - original draft, Writing - review & editing. **Seung-Bum Son**: Data collection. **Marco-Tulio Fonseca Rodrigues**: Experiments, and Writing - original draft, Writing - review & editing, **Juan C. Garcia**: Modeling and Writing - original draft, Writing - review & editing; **Jihyeon Gim**: Experiments, and Writing - original draft, Writing - review & editing; **Kewei Liu**: Writing - review & editing; **Hakim Iddir**: : Modeling, Writing -

review & editing; **Daniel Abraham**: Writing - review & editing; **Zhengcheng Zhang**: Funding support, Writing - review & editing; **Chen Liao**: Supervision, Conceptualization, Funding, Writing - original draft, Writing - review & editing.

Declaration of competing interest

The authors declare that they have no known competing financial interests or personal relationships that could have appeared to influence the work reported in this paper.

Acknowledgement

Support from the Vehicle Technologies Office (VTO), David Howell (Manager), and Battery R&D, Peter Faguy (Technology Manager), at the U.S. Department of Energy, Office of Energy Efficiency and Renewable Energy, is gratefully acknowledged. The electrodes and electrolytes used in this article are from Argonne's Cell Analysis, Modeling and Prototyping Facility. The submitted manuscript has been created by UChicago Argonne, LLC, Operator of Argonne National Laboratory ("Argonne"). Argonne, a U.S. Department of Energy Office of Science laboratory, is operated under Contract No. DE-AC02-06CH11357.

References

1. Jiang, L.; Yu, Y.; Sun, J. Progress of Enhancing the Safety of Lithium Ion Battery from the Electrolyte Aspect. *Nano Energy* **2019**, *55*, 93-114.
2. Feng, X.; Ouyang, M.; Liu, X.; Lu, L.; Xia, Y.; He, X. Thermal Runaway

Mechanism of Lithium Ion Battery for Electric Vehicles: A Review. *Energy Stor. Mater.* **2017**, *10*, 246-267.

3. Tan, S. J.; Yue, J.; Hu, X. C.; Shen, Z. Z.; Wang, W. P.; Li, J. Y.; Zuo, T. T.; Duan, H.; Xiao, Y.; Yin, Y. X.; Wen, R.; Guo, Y. G. Nitriding-Interface-Regulated Lithium Plating Enables Flame-Retardant Electrolytes for High-Voltage Lithium Metal Batteries. *Angew Chem Int Ed Engl* **2019**, *58* (23), 7802-7807.

4. Tan, S-J; Yue, J.; Tian, Y.-F.; Ma, Q.; Wan, J.; Xiao, Y.; Zhang, J.; Yin, Y.-X.; Wen, R.; Xin, S.; Guo, Y.-G. In-Situ Encapsulating Flame-Retardant Phosphate into Robust Polymer Matrix for Safe and Stable Quasi-Solid-State Lithium Metal Batteries. *Energy Stor. Mater.* **2021**, *39*, 186-193.

5. Han, J. G.; Kim, K.; Lee, Y.; Choi, N. S. Scavenging Materials to Stabilize LiPF₆-Containing Carbonate-Based Electrolytes for Li-Ion Batteries. *Adv. Mater.* **2019**, *31* (20), 1804822.

6. Xu, G.; Liu, Z.; Zhang, C.; Cui, G.; Chen, L. Strategies for Improving the Cyclability and Thermo-Stability of LiMn₂O₄-Based Batteries at Elevated Temperatures. *J. Mater. Chem. A* **2015**, *3* (8), 4092-4123.

7. Zhang, S. S.; Jow, T. R. Aluminum Corrosion in Electrolyte of Li-Ion Battery. *J. Power Sources* **2002**, *109* (2), 458-464.

8. Kanamura, K. Anodic Oxidation of Nonaqueous Electrolytes on Cathode Materials and Current Collectors for Rechargeable Lithium Batteries. *J. Power Sources* **1999**, *81-82*, 123-129.

9. Jiang, J.; Dahn, J. R. Effects of Solvents and Salts on the Thermal Stability of LiC₆.

Electrochim. Acta **2004**, *49* (26), 4599-4604.

10. Yu, S.; Lee, C.; Lee, H. Comparative Study on Lithium Borates as Corrosion Inhibitors of Aluminum Current Collector in Lithium Bis(fluorosulfonyl)imide Electrolytes. *J. Power Sources* **2015**, *296*, 197-203.

11. Zhang, Z.; Chen, R.; Li, R.; Lai, R.; Li, R.; Liu, R.; Wang, R. LiPF₆ and Lithium Oxalyldifluoroborate Blend Salts Electrolyte for LiFePO₄/Artificial Graphite Lithium-Ion Cells. *J. Power Sources* **2010**, *195* (21), 7397-7402.

12. Yang, G.; Shi, J.; Shen, C.; Wang, S.; Xia, L.; Hu, H.; Luo, H.; Xia, Y.; Liu, Z. Improving The Cyclability Performance of Lithium-Ion Batteries by Introducing Lithium Difluorophosphate (LiPO₂F₂) Additive. *RSC Adv.* **2017**, *7* (42), 26052-26059.

13. Chengyun, W.; Le, Y.; Weizhen, F.; Jiangwen, L.; Liuzhang, O.; Lichun, Y.; Min, Z. Lithium Difluorophosphate as a Promising Electrolyte Lithium Additive for High-Voltage Lithium-Ion Batteries. *ACS Appl. Energy Mater.* **2018**, *6* (1), 2647-2656.

14. Yang, B.; Zhang, H.; Yu, L.; Fan, W. Z.; Huang, D. Lithium Difluorophosphate as an Additive to Improve the Low Temperature Performance of LiNi_{0.5}Co_{0.2}Mn_{0.3}O₂/Graphite Cells. *Electrochim. Acta* **2016**, 107-114.

15. Choi; Nam-Soon; Jeong; Myung-Hwan; Park; Inbok; Jang; Jun; Yeong; Woo A Combination of Lithium Difluorophosphate and Vinylene Carbonate as Reducible Additives to Improve Cycling Performance of Graphite Electrodes at High Rates. *Electrochem. Commun.* **2015**, *61*, 121-124.

16. Dong, N.; Yang, G.; Luo, H.; Xu, H.; Xia, Y.; Liu, Z. A LiPO₂F₂/LiFSI Dual-Salt Electrolyte Enabled Stable Cycling of Lithium Metal Batteries. *J. Power Sources* **2018**,

400, 449-456.

17. Li, W.; Dolocan, A.; Li, J.; Xie, Q.; Manthiram, A. Ethylene Carbonate-Free Electrolytes for High-Nickel Layered Oxide Cathodes in Lithium-Ion Batteries. *Adv. Energy Mater.* **2019**, *9* (29), 1901152.

18. Long, B. R.; Rinaldo, S. G.; Gallagher, K. G.; Dees, D. W.; Trask, S. E.; Polzin, B. J.; Jansen, A. N.; Abraham, D. P.; Bloom, I.; Bareño, J. Enabling High-Energy, High-Voltage Lithium-Ion Cells: Standardization of Coin-Cell Assembly, Electrochemical Testing, and Evaluation of Full Cells. *J. Electrochem. Soc.* **2016**, *163* (14), A2999-A3009.

19. Tornheim, A.; Peebles, C.; Gilbert, J. A.; Sahore, R.; Garcia, J. C.; Bareño, J.; Iddir, H.; Liao, C.; Abraham, D. P. Evaluating Electrolyte Additives for Lithium-Ion Cells: A New Figure of Merit Approach. *J. Power Sources* **2017**, *365*, 201-209.

20. Yang, J. Z.; Shkrob, I.; Liu, Q.; Rago, N. L. D.; Liu, Y. Z.; Liu, K. W.; Zhang, Z. C.; Liao, C. Structural Underpinnings of Cathode Protection by In Situ Generated Lithium Oxyfluorophosphates. *J. Power Sources* **2019**, 438.

21. Tornheim, A.; Sharifi-Asl, S.; Garcia, J. C.; Bareño, J.; Iddir, H.; Shahbazian-Yassar, R.; Zhang, Z. Effect of Electrolyte Composition on Rock Salt Surface Degradation in NMC Cathodes During High-Voltage Potentiostatic Holds. *Nano Energy* **2019**, *55*, 216-225.

22. Petibon, R.; Xia, J.; Ma, L.; Bauer, M. K. G.; Nelson, K. J.; Dahn, J. R. Electrolyte System for High Voltage Li-Ion Cells. *J. Electrochem. Soc.* **2016**, *163* (13), A2571-A2578.

23. Ma, L.; Glazier, S. L.; Petibon, R.; Xia, J.; Peters, J. M.; Liu, Q.; Allen, J.; Doig, R. N. C.; Dahn, J. R. A Guide to Ethylene Carbonate-Free Electrolyte Making for Li-Ion Cells. *J. Electrochem. Soc.* **2017**, *164* (1), A5008-A5018.
24. Gachot, G.; Grugeon, S.; Armand, M.; Pilard, S.; Guenot, P.; Tarascon, J. M.; Laruelle, S. Deciphering the Multi-Step Degradation Mechanisms of Carbonate-Based Electrolyte in Li Batteries. *J. Power Sources* **2008**, *178* (1), 409-421.
25. Grützke, M.; Kraft, V.; Weber, W.; Wendt, C.; Friesen, A.; Klamor, S.; Winter, M.; Nowak, S. Supercritical Carbon Dioxide Extraction of Lithium-Ion Battery Electrolytes. *J. Supercrit. Fluids* **2014**, *94*, 216-222.
26. Sasaki, T.; Abe, T.; Iriyama, Y.; Inaba, M.; Ogumi, Z. Suppression of an Alkyl Dicarboxylate Formation in Li-Ion Cells. *J. Electrochem. Soc.* **2005**, *152* (10), A2046.
27. Qian, Y.; Hu, S.; Zou, X.; Deng, Z.; Xu, Y.; Cao, Z.; Kang, Y.; Deng, Y.; Shi, Q.; Xu, K.; Deng, Y. How Electrolyte Additives Work in Li-Ion Batteries. *Energy Storage Mater.* **2019**, *20*, 208-215.
28. Yang, J. Z.; Shkrob, I.; Liu, K. W.; Connell, J.; Rago, N. L. D.; Zhang, Z. C.; Liao, C. 4-(Trimethylsilyl) Morpholine as a Multifunctional Electrolyte Additive in High Voltage Lithium Ion Batteries. *J. Electrochem. Soc.* **2020**, *167* (7).
29. Su, C. C.; He, M.; Amine, R.; Chen, Z.; Sahore, R.; Rago, N. D.; A, K. A. Cyclic Carbonate for Highly Stable Cycling of High Voltage Lithium Metal Batteries. *Energy Storage Mater.* **2019**, *17*, 284-292.
30. Wang, A.; Kadam, S.; Li, H.; Shi, S.; Qi, Y. Review on Modeling of the Anode Solid Electrolyte Interphase (SEI) for Lithium-Ion Batteries. *Npj Comput. Mater.* **2018**,

4 (1), 15.

31. Ohzuku, T.; Ueda, A.; Nagayama, M. Electrochemistry and Structural Chemistry of LiNiO₂ (R3m) for 4 Volt Secondary Lithium Cells. *J. Electrochem. Soc.* **1993**, *140* (7), 1862-1870.

32. Yoon, C. S.; Jun, D.-W.; Myung, S.-T.; Sun, Y.-K. Structural Stability of LiNiO₂ Cycled above 4.2 V. *ACS Energy Lett.* **2017**, *2* (5), 1150-1155.

33. Dahn, H. M.; Smith, A. J.; Burns, J. C.; Stevens, D. A.; Dahn, J. R. User-Friendly Differential Voltage Analysis Freeware for the Analysis of Degradation Mechanisms in Li-Ion Batteries. *J. Electrochem. Soc.* **2012**, *159* (9), A1405-A1409.

For Table of Contents Only

